

DeLiO: Decoupled LiDAR Odometry

Queens Maria Thomas¹ Oliver Wasenmüller¹ Didier Stricker¹

Abstract—Most LiDAR odometry algorithms estimate the transformation between two consecutive frames by estimating the rotation and translation in an intervening fashion. In this paper, we propose our Decoupled LiDAR Odometry (DeLiO), which – for the first time – decouples the rotation estimation completely from the translation estimation. In particular, the rotation is estimated by extracting the surface normals from the input point clouds and tracking their characteristic pattern on a unit sphere. Using this rotation the point clouds are unrotated so that the underlying transformation is pure translation, which can be easily estimated using a line cloud approach. An evaluation is performed on the KITTI dataset and the results are compared against state-of-the-art algorithms.

I. INTRODUCTION

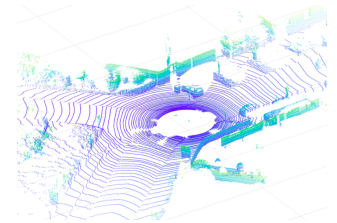
Odometry plays an essential role in many applications such as robot navigation or autonomous driving where robust and precise estimation of the trajectory is a main challenge. Nowadays, this has become more interesting as a variety of sensors that could include the spatial information as well have emerged [1]. A LiDAR (Light Detection And Ranging) is such an active optical sensor that can provide highly accurate range measurements where errors are usually constant irrespective of the distance.

Odometry is often estimated by incrementally integrating the relative transformations resulting from consecutive point cloud registrations. Traditional point cloud registration approaches such as Iterative Closest Point [2], [3] alternate between the translation and rotation estimation in an iterative fashion. This has the overhead of estimating the three degrees of translational freedom and three degrees of rotational freedom simultaneously. In this paper, we propose the new DeLiO algorithm that estimates the transformation by decoupling the rotation from translation and thus making the six DoF odometry estimation boil down to two times three DOF. To the best of our knowledge, we are the first to propose this decoupling for LiDAR odometry.

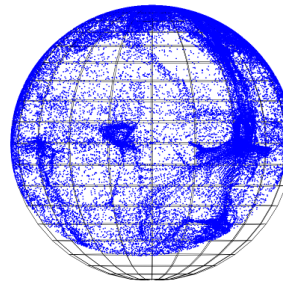
The decoupling of rotation estimation in DeLiO is driven by the following main observation in two consecutive LiDAR point clouds: The rotational difference between surface normals corresponds to the rotation difference between their corresponding LiDAR scans. This property is independent of any translation, since translation does not affect the surface normals. Thus, this can be exploited to estimate the rotation independent of translation. The main challenge in DeLiO is to determine the rotation difference in the normals of two LiDAR scans. In Section III we propose a new approach to track these surface normals over time. Later,



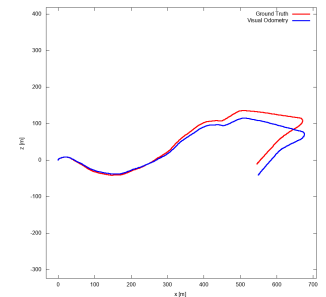
(a) LiDAR scanner



(b) LiDAR point cloud



(c) Normals on unit sphere



(d) DeLiO trajectory

Fig. 1. In this paper, we propose DeLiO – a LiDAR odometry decoupling rotation from translation estimation. Decoupling is achieved by tracking surface normals on a unit sphere for rotation estimation, which is independent of translation estimation.

point clouds are unrotated using the estimated rotation so that the underlying transformation is a pure translation. This translation is estimated in Section IV using a state-of-the-art line cloud odometry inspired from the work of Velas et al. [4]. In Section VI we verify the state-of-the-art performance of DeLiO on the KITTI benchmark. An overview of our new approach is given in Figure 2.

II. RELATED WORK

In the literature plenty of odometry algorithms exist for several visual sensor types [5]. Several algorithms – such as LIMO [6], DEMO [7], etc. – estimate the odometry out of a monocular or stereo camera and use the LiDAR points for support only. However, for our approach we want to rely on pure LiDAR information.

Since LiDAR information is a large-scale point cloud, point cloud registration is usually applied in the state-of-the-art for LiDAR-only odometry. For point cloud registration often variations of the traditional Iterative Closest Point (ICP) [3] are utilized. ICP and its variations estimate the transformation involved between two scans by iteratively estimating rotation and translation in an alternating fashion. But, ICP is prone to local minima when the point clouds

¹German Research Center for Artificial Intelligence - DFKI, Kaiserslautern, Germany, `firstname.lastname@dfki.de`

are considerably far from each other. This is because the point cloud correspondences can be accurately estimated only when initial alignment is already very good. Also ICP is highly sensitive to noise and outliers. The exact point to point matching in standard ICP does not take into account the differential sampling of the two point clouds and thus may lead to pairs without good equivalence. A few ICP variants were proposed to overcome this issue by taking information from surface normals into consideration. Two prominent variants are *Point-To-Plane* approach that considers the surface normals from the target point cloud only and *Plane-To-Plane* variant that uses the normals from both source and target point cloud.

A recent state-of-the-art approach in odometry using LiDAR sensors is LiDAR Odometry and Mapping in Real-time (LOAM) [8] that extracts features that are on sharp edges and planar surface patches using the scan sweep information. Also, LOAM integrates data from IMU units as well to improve the accuracy of estimation. Visual-LOAM (V-LOAM) [9], is a variation of LOAM that aims at motion estimation and mapping using a monocular camera with a 3D LiDAR instead of IMU. A recent variation of ICP is Implicit Moving Least Squares-SLAM (IMLS) [10], that relies on a scan-to-model matching framework. Initially the LiDAR scans are sampled with a sampling strategy and then a model is defined from the previous localized LiDAR sweeps and use an Implicit Moving Least Squares (IMLS) surface representation. Unlike LOAM, IMLS does not use any data from other sensors like IMU or cameras but removes dynamic objects from the scene as a pre-processing step. The DLO [11] approach estimates the odometry directly, by projection the LiDAR scan to a ground plane and registering the resulting grid maps.

Unlike the before mentioned approaches, our method DeLiO decouples for the first time the rotation completely from translation in LiDAR odometry. Thus, rotation can be estimated in one step. The point clouds are later unrotated with the estimated rotation so that the underlying transformation is pure translation, which is estimated using a modified line cloud odometry. A further refinement of the rotation is no longer necessary in comparison to the state-of-the-art algorithms. Also DeLiO does not use any data from other sensors like IMU, cameras or GPS.

III. ROTATION ESTIMATION

DeLiO determines odometry by decoupling rotation from translation estimation. Thus, a robust rotation estimation scheme is necessary, which can be estimated independently of the translation. Utilizing the 3D coordinates captured by the LiDAR scanner directly is not feasible, since their alignment involves rotation as well as translation.

Therefore, our main idea is to use the surface normals of the captured LiDAR scans for rotation estimation. Surface normals can be extracted directly from the captured scans and convey rich geometric information. The normal vector distributions typically contain a characteristic structure depending on the captured environment as visible in Figure

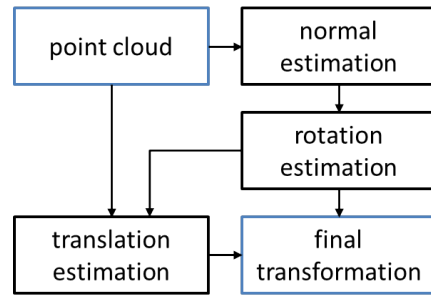


Fig. 2. Overview of DeLiO: Normals are extracted out of the input point clouds and rotation is estimated independently of translation. Translation is estimated out of the unrotated point clouds.

3. These structural regularities lead to robust patterns in the normal vector density distribution. The rotational difference between two subsequent patterns corresponds to the rotation difference between their corresponding LiDAR scans. Thus, we track the normal distribution over time in order to determine rotation. This can be done completely independent of the translation difference.

In the following, our new rotation approach for DeLiO is described in more detail. We start with the normal extraction out of the captured LiDAR scans. In order to distinguish characteristic patterns in the normal distribution from random noise, we apply a statistical outlier filtering. If the retained subset is not enough for a pattern registration, a mean shift seeking is performed to extract more patterns from the surface normals. Later rotation is estimated out of the displacement of these patterns using a Singular Value Decomposition (SVD).

A. Surface Normal Extraction

Surface normals are extracted, since they are translation independent geometric properties. A least-square plane fitting estimation problem [12] that estimates the normal of a point on a surface by approximating the normal of a plane tangent to the surface is used for surface normal estimation. The analysis of eigenvectors and eigenvalues (estimated using Principal Component Analysis (PCA) [13]) of a covariance matrix formulated from the k -nearest neighbors [14] of each query point helps in estimating the surface normals corresponding to the query points. The covariance matrix is formulated as

$$C = \frac{1}{k} \sum_{i=1}^k \cdot (p_i - \bar{p}) \cdot (p_i - \bar{p})^T, \quad C \cdot \vec{v}_j = \lambda_j \cdot \vec{v}_j, \quad (1)$$

where k is the number of nearest neighbors of point p_i , \bar{p} is the centroid of the k nearest neighbors of p_i , and \vec{v}_j is the j -th eigenvector of the covariance matrix, and λ_j is the j -th eigenvalue. In order to be more robust against outliers, bilateral filtering on the surface normals is applied [15].

Prominent aspects from the surface normals are now identified by analyzing the pattern formed by these normals on an unit sphere. The motivation behind this idea is the fact that the resulting characteristic pattern on unit sphere is

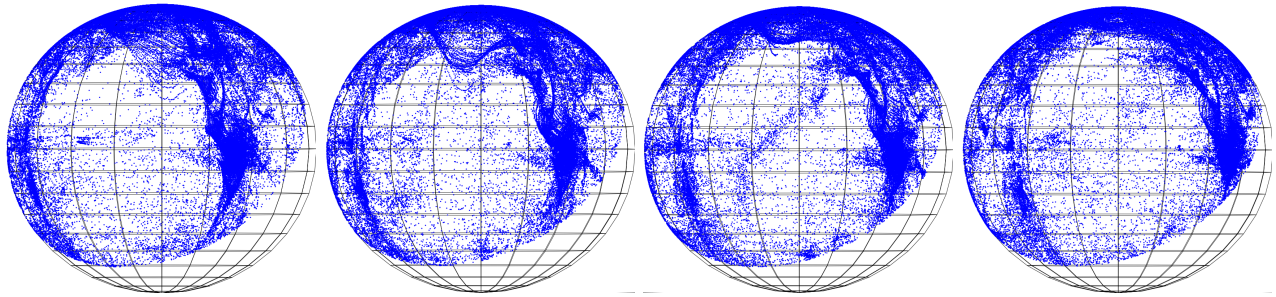


Fig. 3. Surface normal mapping on the unit sphere for four consecutive frames. A characteristic pattern is moving over the unit sphere over time. This rotational movement corresponds to the rotation between the corresponding LiDAR scans, independent of the translation.

moving over the unit sphere over time as depicted in Figure 3. Tracking this pattern over time yields rotation independent of translation.

B. Statistical Outlier Removal

The presence of large number of scattered points on the unit sphere affects adversely the tracking of the pattern. Hence a robust outlier removal scheme has to be considered to select a subset of the points on the unit sphere that effectively represent the underlying pattern.

Therefore, we utilize a statistical outlier removal scheme [16] that performs a statistical analysis in the neighborhood of each point, removing those points violating a certain criteria. For every point the mean distance to all its neighbors are calculated. Under the assumption that the resulting distribution is Gaussian with a mean and standard deviation, all points whose mean distances are outside a defined interval are considered as outliers and removed. Considering various number of neighboring points, this is done iteratively to retain a small but stable set of points. The resulting surface normals on the unit sphere are shown in Figure 4.

If the scene lacks significant characteristic features, the resulting pattern on the unit sphere may be sparse and does not convey meaningful information to estimate the rotation. If the number of points retained after statistical outlier removal is lower than a threshold value, the may mean that the only remaining points represent ground because of the large number of ground points resulting in very dense areas over the unit sphere. A mean shift seeking [17] explained in detail in the following section is used if the retained number of points fall below a certain threshold value. This would facilitate finding more structures or dense points corresponding to new structures other than ground. Once the dense positions are discovered, a ball query discovers neighbors in a certain radius around each of the dense points. Since these points are prone to outliers or noise, statistical outlier removal is performed until a good number of points remain. The obtained points are downsampled and filtered using uniform sampling. Here a 3D voxel grid is assembled over the input points and in each voxel, all the points are assumed with their centroid. This approach reduces the number of points significantly, retaining only the best points and no outliers.

C. Mean Shift Seeking

As explained before, in case too few normals are retained after the Statistical Outlier Removal, a mean shift seeking is applied in order to preserve also fine structures for normal tracking. The mean shift seeking procedure applies local Kernel Density Estimation (KDE), if an initial approximate location of the mode is known and takes steps iteratively in the direction of increasing density. To ensure that the whole surface of the sphere is covered, the sphere surface is divided into a grid of uniform size which gives a set of coordinates that can be used to initialize the mode seeking. A nearest neighbor approach was used to clean the identified set of modes since mean shift iterations may converge to same modes if the initialization points are close to each other. The idea is to perform a single mean shift iteration for each mode given a subset of normal vectors on unit sphere. The subset is selected by considering all normal vectors that are in the neighborhood of considered center f_j . The range of the neighborhood is a conical window centered at the center of the sphere with an apex angle of θ_{window} . The required subset of normal vectors n_i lie within this conical window and satisfies the condition

$$\|n_i \times f_j\| < \sin(\theta_{window}/2). \quad (2)$$

To compute the mean shift, these normal vectors are then projected into the tangential plane at f_j . A Riemann exponential map [18] is applied so that the projected vectors represent proper angular deviations in the tangential plane. Then the mean shift in the tangential plane is computed as

$$S'_j = \frac{\sum_{ij} e^{-c\|m'_{ij}\|^2} m'_{ij}}{\sum_{ij} e^{-c\|m'_{ij}\|^2}}, \quad (3)$$

where m'_{ij} are the tangential plane coordinates. c is a design parameter that defines the width of the kernel in the tangential plane and can be derived from θ_{window} . The mean shift after computation is transformed onto the unit sphere again using Riemann logarithmic map.

D. Pattern Registration

Finally, rotation is estimated using a Singular Value Decomposition (SVD) [19]. For each target point, the corresponding source point is obtained using a k-nearest neighbor

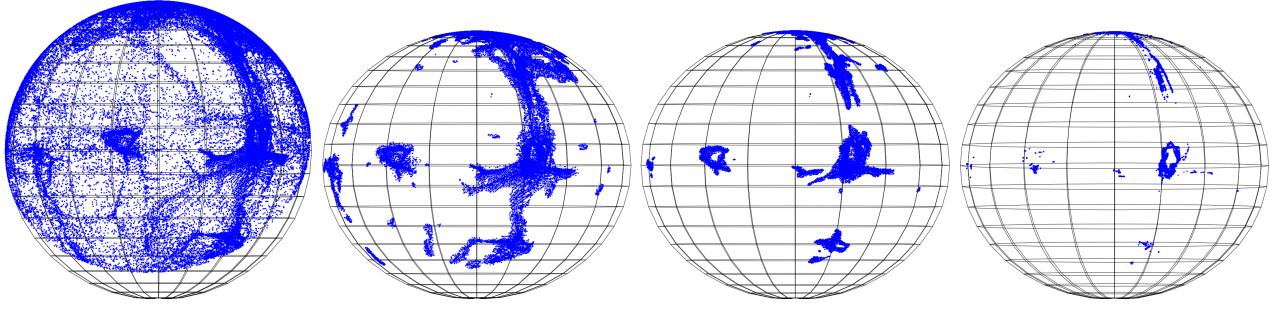


Fig. 4. Statistical Outlier Removal (SOR) applied iteratively (from left to right) on the unit sphere of surface normals.

method. A KD-Tree [14] is constructed using the source point set and thus reducing the search space significantly. Once the correspondences are obtained, SVD can be used to estimate rotation. This is performed iteratively till estimated rotation converges. Using our new described approach makes it possible to estimate rotation completely independent from translation. Also an alternation between rotation and translation estimation is not necessary, since the final rotation is estimated after executing the procedure explained in this Section.

IV. TRANSLATION ESTIMATION

After the rotation is estimated, this result can be used to unrotate the two LiDAR scans. The remaining transformation between them is then a pure translation. A major problem involved in LiDAR point cloud registration is the sparsity of the point cloud. Also the ring structure of the point cloud leads to incorrect registration [4]. Since classical ICP approaches [2], [3] try to minimize the distance of closest points, the resulting transformation could be the one that fits the ring structures that represent the floor because of the larger number of floor ring points. These issues associated with point clouds can be effectively handled by a line cloud proposed by Velas et al. [4]. In contrast to their algorithm where rotation and translation are estimated simultaneously, we use this approach for translation estimation only.

The line cloud approach has two main parts. First, the points in the point cloud are transformed into polar coordinate system and line cloud is generated. Second, the generated lines are registered and translation is obtained by aligning the centroids. Conversion to line cloud addresses the sparsity issue of the point cloud by generating lines such that the lines represent the underlying scene geometry efficiently. The original point cloud is iteratively resampled so that the new points for registration do not come from the point cloud, but the closest points between two matching pair of lines.

A. Line Cloud Generation

As an initial step, each 3D point is converted from Cartesian coordinate system to a polar coordinate system for the line cloud generation. A polar coordinate system is a two dimensional coordinate system where each point is determined by a distance, r from the origin (radial coordinate) and an angle, θ from the reference direction (angular

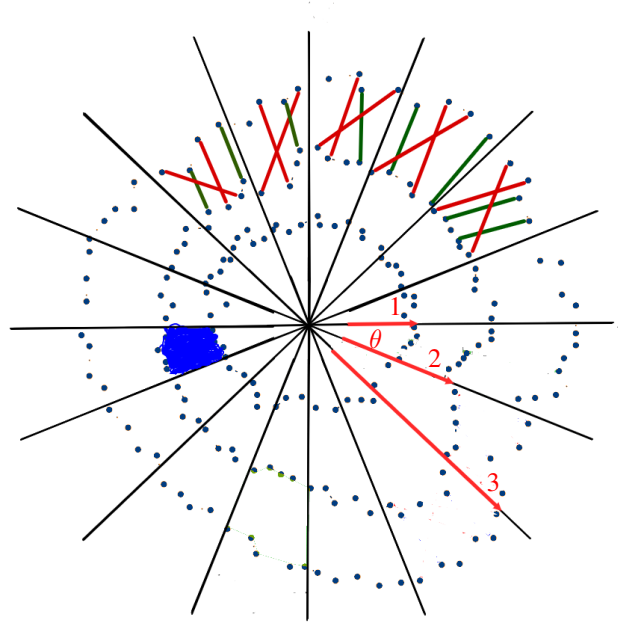


Fig. 5. Line Cloud generation [4]: The area around the LiDAR scanner is divided into rings and bins so that the points are represented in polar coordinate system. One sample bin is shown in blue color. Lines (red and green) are drawn connecting points in consecutive rings and bins. Only shortest lines (green) are preserved.

coordinate). The Cartesian coordinates $[x,y,z]$ of the point cloud can be converted to polar coordinates r and θ by

$$r = \sqrt{x^2 + y^2} \quad \theta = \text{atan2}(y, x) \quad \theta \in [0, 360), \quad (4)$$

where θ is the angle within ground plane $x-y$ and r represents the distance from origin. Vertical axis z is not considered for the conversion because of the horizontal ring layout of the point cloud.

The LiDAR scanner produces rays such that each ray captures a ring of points as depicted by the red arrows in Figure 5. Points in the point cloud are shown as blue dots. Line cloud is generated by connecting some of the promising points in the point cloud in such a way that the underlying local surface properties are captured. The scanner position is considered as origin and the space around is divided into polar bins. Each point in the point cloud is represented by the ring and bin. One sample bin is shown by blue color

in Figure 5. To ensure points of similar angle are selected, random lines are generated in each bin connecting points from consequent rings. Only few promising points from the line cloud are selected using a filtering criteria. Preserving only shorter lines (green lines) ensures that real planes are connected and points connecting different planes (red lines) are discarded.

B. Line Cloud Registration

Once the point cloud is sampled into line cloud, the translation is estimated using a variation of ICP. Since the point clouds are unrotated with absolute rotation, translation is calculated iteratively by finding closest matches from the line cloud. Instead of finding point-to-point correspondences, the algorithm finds correspondences between source and target line segments. This is done by finding the line segment in the target cloud whose center is close to the center of source line segment using a KD-Tree implementation. A distance threshold is included to eliminate incorrect matches in such a way that only the source and target line center pairs whose distance is less than the mean distance of all match pairs are kept.

Once the matching pair of line segments are found out, the line segments are aligned into a 3D plane that gives the translation involved. Consider a matching pair of lines l_s and l_t that are taken from the source cloud and target cloud respectively. The parametric representation of the lines given 3D points P_{s0} and P_{t0} and vectors u_s and u_t are

$$l_s : P_s = P_{s0} + t_s \cdot u_s; \quad t_s \in (-\infty, \infty) \quad (5)$$

$$l_t : P_t = P_{t0} + t_t \cdot u_t; \quad t_t \in (-\infty, \infty), \quad (6)$$

where u_s and u_t are vectors representing the direction of the line segments.

In any n dimensional space, the two lines l_s and l_t are closest at points X_s and X_t when w is the unique minimum of $w(P_s, P_t)$ [20]. These closest points X_s and X_t are the correspondences between the source and target line clouds. The closest points between these lines are given by

$$X_s = P_{s0} + t_{sc} \cdot u_s \quad (7)$$

$$X_t = P_{t0} + t_{tc} \cdot u_t \quad , \quad (8)$$

where,

$$t_{sc} = \frac{be - cd}{ac - b^2} \quad t_{tc} = \frac{ae - bd}{ac - b^2} \quad (9)$$

$$a = u_s \cdot u_s \quad b = u_s \cdot u_t \quad c = u_t \cdot u_t \quad (10)$$

$$d = u_s \cdot w \quad e = u_t \cdot w \quad w = P_{s0} - P_{t0} \quad (11)$$

The final transformation is estimated from the centroids of both sets of points under the assumption that the underlying transformation is pure translation. When the line clouds are registered, the distance between the preserved lines become very small or close to zero and the lines are coplanar.

V. OPTIMIZATION

Odometry integrates small relative transformations incrementally over time. The incremental nature of this estimation is subject to drift that accumulates to large errors [21] This drift can be reduced to a certain extend using a variety of optimization techniques. Estimated transformations can be improved using multi-frame processing [22] as well as prediction based on constant velocity motion model.

Since DeLiO relies on a tracking of the surface normals for rotation estimation, a good initialization is beneficial. The closer the prediction is to the actual rotation value, the better is the final rotation result. Thus, we use a linear prediction model. The prediction T_p for pairs of frames at time i and $i + 1$ can be estimated from previous N frames using the linear prediction as

$$T_p = \frac{2}{N(N+1)} \sum_{j=1}^N (N-j+1) T_{i-j}. \quad (12)$$

Even though prediction improves results considerably, there is increased accumulation of drift as the length of trajectory increases. A recent trend is to use graphical models [23] to solve the accumulated drift through optimization. One way of formulating a pose-graph for optimization is to construct a graph whose nodes correspond to the poses of the sensor at different points in time and whose edges represent constraints between the poses. The constructed pose-graph can be further optimized by minimizing a non-linear error function that corresponds to the graph.

Graph based optimization approaches build a pose graph incrementally taking the sensor pose at each point of time. The first node is constructed using the initial pose of the sensor. As soon as the sensor moves to a new position, the transformation between these positions is computed using the DeLiO algorithm of Sections III and IV. When this transformation is applied to position a , a new measurement at position $a + 1$ is acquired. The edge between positions a and $a + 1$ correspond to this estimated transformation. When the car moves further, a new transformation is available which when applied to position $a + 1$ gives measurement at position $a + 2$. The transformation between position a and $a + 2$ can be estimated if a sufficient overlap exists between these two positions. A third edge may be added between position a and $a + 2$ in the pose-graph. Due to imperfections in the incremental registration and noise from the environment, the two estimations at position $a + 2$ may differ a bit. This error can be minimized by fine tuning the graph using optimization algorithms that update the pose with the optimized values.

Before optimization, an error function needs to be defined. A non linear least squares optimization can be described by

$$F(x) = \sum_{\langle k \rangle \in \mathcal{C}} \underbrace{e(x_k, z_k)^\top \Omega_k e(x_k, z_k)}_{F_k} \quad (13)$$

$$x^* = \underset{x}{\operatorname{argmin}} F(x), \quad (14)$$

where x is a vector of parameters. z_k and Ω_k represent the mean and information matrix relating the parameters in

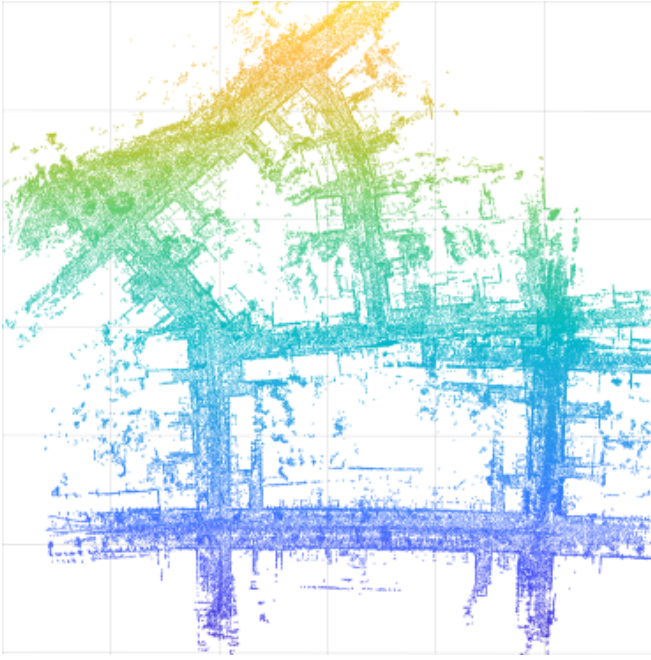


Fig. 6. Example of environment map (KITTI *training* sequence #07) utilizing the DeLiO trajectory.

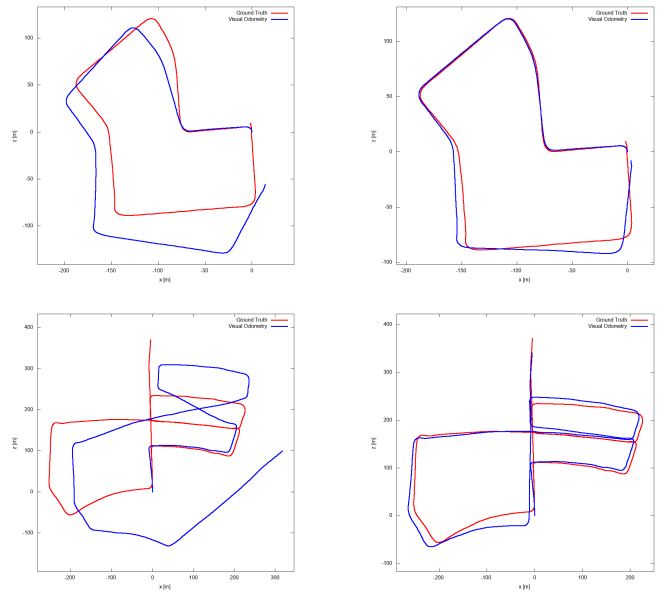
x_k . $e(x_k, z_k)$ defines how well the parameters x_k fits the constraints in z_k and Ω_k . The information matrix contains value indicating how good the current measurement is. This is the inverse of covariance matrix. The Levenberg-Marquardt algorithm [24] implemented in g^2o [25] is used to carry out the optimizations.

VI. EVALUATION

For evaluation of our new DeLiO approach, we use the KITTI [26] odometry benchmark. This dataset consists of 22 sequences out of which 11 sequences have ground truth trajectories available for training. The benchmark includes monochromatic and color image sequences, GPS-IMU data and laser scanner data collected in both urban and rural areas of City of Karlsruhe, Germany. For our work we utilize the laser scanner data only; all other data is neglected. The laser scanner data is represented as a point cloud acquired by a Velodyne HDL-64E LiDAR. The evaluation metrics suggested by KITTI compute the rotation and translation errors separately by evaluating errors as a function of the trajectory length and velocity .

Final transformation is computed by combining the rotation (see Section III) and translation (see Section IV) as well as an optimization of this transformation (see Section V). When concatenating the relative transformations between scans, a long trajectory of the full sequence can be created as exemplary visible in Figure 7 and the supplementary video ¹. The estimated transformation can also be applied over time to the point clouds resulting in an environment map. Figure 6 shows such an environmental map formulated for sequence #07 validating the functionality of DeLiO.

¹<https://youtu.be/HzwwxQfpKNo>



(a) unoptimized DeLiO

(b) optimized DeLiO

Fig. 7. Estimated trajectories of *training* sequence #07 (top) and #05 (bottom) with and without optimization (cp. Section V). Ground truth is plotted in red and our estimated DeLiO trajectory in blue.

Figure 7 shows two trajectories corresponding to sequences #07 and #05 before and after optimization (cp. Section V). Unoptimized trajectory errors are resulting from few erroneous registration caused due to overturning vehicles, pedestrians and other dynamic objects in the scene. Lack of characteristic features in the scene can also introduce errors. Since odometry accumulates small transformations over time, few erroneous frames may result in significant drift towards the end of the trajectory. This is reduced to a certain extend using a linear motion model and pose graph optimization.

In Figure 8 the state-of-the-art algorithms are compared against DeLiO in a ground truth comparison of their trajectories. While BCC and BLO [27] show a strong drift, DeLiO demonstrates similar accuracy to DEMO [7], LIMO [6] and SuMa [28]. This verifies the state-of-the-art performance of our new decoupling approach.

Table I shows a quantitative comparison of DeLiO with the state-of-the-art approaches. It is important to know that the better performing algorithms utilize additional sensor information or special pre-processing. For example, LOAM [8] integrates IMU data for rotation estimation, whereas IMLS [10] pre-processes the LiDAR scans to remove dynamic objects from the scene. LIMO [6] and DEMO [7] utilize additional color information. Our proposed approach DeLiO uses only LiDAR data without removing the dynamic objects and without using any loop detection. The stated error in Table I results from very few erroneous registrations leading to the increased average value. Erroneous registration is caused due to overturning vehicles, pedestrians and other dynamic objects in the scene. A vehicle moving close to

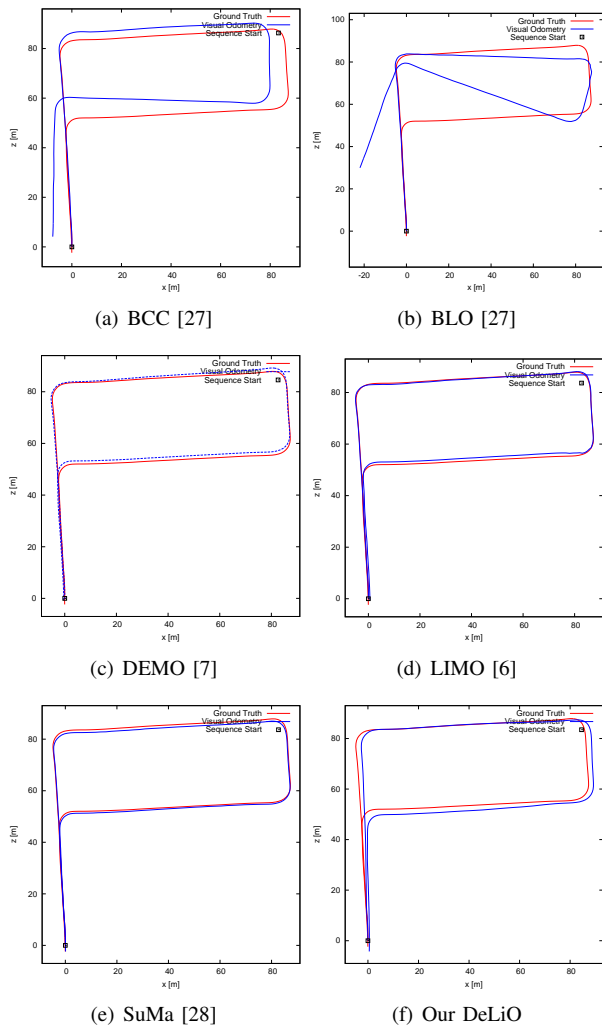


Fig. 8. Comparison of our DeLiO against state-of-the-art approaches on KITTI test sequence #14.

the sensor can result in clusters over the unit sphere. Since the algorithm retains only the major clusters/dense regions and rejects everything else from the scene as outliers, the registration may introduce large error and can affect the whole odometry. Those frames with no characteristic patterns can also cause substantial errors because of the lack of clusters or reasonable patterns on the unit sphere. This is reduced using the optimization techniques. Other challenges include relatively high car speed, where the sequences are recorded at 10 fps.

VII. CONCLUSION

This paper presents a new algorithm called DeLiO for odometry using LiDAR point clouds by decoupling rotation from translation. The rotation estimation approach based on the distribution pattern of surface normals on unit sphere is independent of translation and thus stands out from the state-of-the-art approaches. To the best of our knowledge, we are the first presenting such an approach for LiDAR odometry. In the evaluation we showed the effectiveness of DeLiO on the well-known KITTI benchmark. In order to achieve

Method	Avg trans err	Avg rot err
LOAM [8]	0.59%	0.0014[d/m]
IMLS [10]	0.64%	0.0016[d/m]
DEMO [7]	1.14%	0.0049[d/m]
SuMA [28]	1.39%	0.0034[d/m]
BCC [27]	4.59%	0.0175[d/m]
DeLiO (our)	5.32%	0.0213[d/m]
NCICP	7.17%	0.0050[d/m]
BLO [27]	9.21%	0.0163[d/m]

TABLE I

COMPARISON OF DELIO WITH STATE-OF-THE-ART METHODS. DELIO IS SHOWING COMPARABLE RESULTS USING LiDAR SCANS ONLY.

even better results on the benchmark further engineering is necessary.

Consequentially, as future work it will be interesting to remove the dynamic objects from the scenes as proposed in [10]. These dynamic objects are contributing a lot to rotational error. For the detection of dynamic objects, optical flow [29] or scene flow [30] algorithms could be utilized. Also objects that are observed in one frame and not in another may also be removed to improved the performance. Another potential improvement would be to consider a new place recognition algorithm for loop closure like SegMatch [31]. Detected loop closures could be easily integrated into the already used pose graph and considered for optimization.

REFERENCES

- [1] T. Yoshida, O. Wasenmüller, and D. Stricker, "Time-of-flight sensor depth enhancement for automotive exhaust gas," in *IEEE International Conference on Image Processing (ICIP)*. IEEE, 2017, pp. 1955–1959.
- [2] P. J. Besl and N. D. McKay, "Method for registration of 3-d shapes," in *Sensor Fusion IV: Control Paradigms and Data Structures*. International Society for Optics and Photonics, 1992.
- [3] Y. He, B. Liang, J. Yang, S. Li, and J. He, "An iterative closest points algorithm for registration of 3d laser scanner point clouds with geometric features," 2017.
- [4] M. Velas, M. Spanel, and A. Herout, "Collar line segments for fast odometry estimation from velodyne point clouds," in *IEEE International Conference on Robotics and Automation (ICRA)*, 2016.
- [5] G. Dudek and M. Jenkin, *Inertial sensors, GPS, and odometry*. Springer, 2008.
- [6] J. Graeter, A. Wilczynski, and M. Lauer, "Limo: Lidar-monocular visual odometry," in *IEEE/RSJ International Conference on Intelligent Robots and Systems (IROS)*. IEEE, 2018.
- [7] J. Zhang, M. Kaess, and S. Singh, "Real-time depth enhanced monocular odometry," in *IEEE/RSJ International Conference on Intelligent Robots and Systems (IROS)*. IEEE, 2014.
- [8] J. Zhang and S. Singh, "Loam: Lidar odometry and mapping in real-time," in *Robotics: Science and Systems Conference*, 2014.
- [9] J. Zhang and Singh, "Visual-lidar odometry and mapping: Low-drift, robust, and fast," *IEEE International Conference on Robotics and Automation (ICRA)*, 2015.
- [10] J.-E. Deschaud, "Imls-slam: scan-to-model matching based on 3d data," *arXiv preprint arXiv:1802.08633*, 2018.
- [11] L. Sun, J. Zhao, X. He, and C. Ye, "Dlo: Direct lidar odometry for 2.5 d outdoor environment," in *IEEE Intelligent Vehicles Symposium (IV)*. IEEE, 2018.
- [12] R. B. Rusu, "Semantic 3d object maps for everyday manipulation in human living environments," Ph.D. dissertation, Technische Universität München (TUM), Germany, 2009.
- [13] I. Jolliffe, *Principal Component Analysis*. Springer Verlag, 1986.
- [14] M. Otair, "Approximate k-nearest neighbour based spatial clustering using k-d tree," 2013.

- [15] O. Wasenmüller, G. Bleser, and D. Stricker, “Combined bilateral filter for enhanced real-time upsampling of depth images,” in *International Conference on Computer Vision Theory and Applications (VISAPP)*, 2015.
- [16] “Point Cloud Library (PCL). removing outliers using a statistical outlier removal filter,” Available online: <http://pointclouds.org/>, accessed: 2014-07-03.
- [17] M. A. Carreira-Perpinán, “A review of mean-shift algorithms for clustering,” *arXiv preprint arXiv:1503.00687*, 2015.
- [18] J. Straub, G. Rosman, O. Freifeld, J. Joseph Leonard, and J. W. Fisher III, “A mixture of manhattan frames: Beyond the manhattan world,” in *IEEE Conference on Computer Vision and Pattern Recognition (CVPR)*, 2014.
- [19] D. Kalman, “A singularly valuable decomposition: The svd of a matrix,” *College Math Journal*, 1996.
- [20] J. Olive, *Maths. A student's survival guide. A self-help workbook for science and engineering students*. Cambridge University Press, Cambridge, 2003.
- [21] H. Liu, R. Jiang, W. Hu, and S. Wang, “Navigational drift analysis for visual odometry,” *Computing and Informatics*, 2015.
- [22] H. Badino, A. Yamamoto, and T. Kanade, “Visual odometry by multi-frame feature integration,” in *International Workshop on Computer Vision for Autonomous Driving @ ICCV*, December 2013.
- [23] G. Grisetti, R. Kummerle, C. Stachniss, and W. Burgard, “A tutorial on graph-based slam,” *IEEE Intelligent Transportation Systems Magazine*, 2010.
- [24] R. I. Hartley and A. Zisserman, *Multiple View Geometry in Computer Vision*, 2nd ed. Cambridge University Press, ISBN: 0521540518, 2004.
- [25] R. Kümmerle, G. Grisetti, H. Strasdat, K. Konolige, and W. Burgard, “g 2 o: A general framework for graph optimization,” in *IEEE International Conference on Robotics and Automation (ICRA)*, 2011.
- [26] A. Geiger, P. Lenz, C. Stiller, and R. Urtasun, “Vision meets robotics: The kitti dataset,” *The International Journal of Robotics Research*, 2013.
- [27] M. Velas, M. Spänzel, M. Hradis, and A. Herout, “Cnn for imu assisted odometry estimation using velodyne lidar,” *arXiv preprint arXiv:1712.06352*, 2017.
- [28] J. Behley and C. Stachniss, “Efficient surfel-based slam using 3d laser range data in urban environments,” in *Robotics: Science and Systems (RSS)*, 2018.
- [29] R. Schuster, Bailer, O. Wasenmüller, and D. Stricker, “Flowfields++: Accurate optical flow correspondences meet robust interpolation,” in *IEEE International Conference on Image Processing (ICIP)*. IEEE, 2018, pp. 1463–1467.
- [30] R. Schuster, C. Bailer, O. Wasenmüller, and D. Stricker, “Combining stereo disparity and optical flow for basic scene flow,” in *Commercial Vehicle Technology 2018*. Springer, 2018, pp. 90–101.
- [31] R. Dubé, D. Dugas, E. Stumm, J. Nieto, R. Siegwart, and C. Cadena, “Segmatch: Segment based place recognition in 3d point clouds,” in *IEEE International Conference on Robotics and Automation (ICRA)*, 2017.